Talanta 175 (2017) 382–389

Contents lists available at ScienceDirect

Talanta

journal homepage: www.elsevier.com/locate/talanta

Highly sensitive amperometric biosensor for determination of NADH and ethanol based on Au-Ag nanoparticles/poly(L-Cysteine)/reduced graphene oxide nanocomposite

Gözde Aydoğdu Tığ

Biochemistry Division, Department of Chemistry, Faculty of Science, Ankara University, 06100 Ankara, Turkey

ARTICLE INFO

Keywords:
NADH determination
Alcohol dehydrogenase
Au-Ag nanoparticles
Poly(L-cysteine)
Reduced graphene oxide

ABSTRACT

This work presents the fabrication of a novel nicotinamide adenine dinucleotide (NADH) sensor using gold-silver bimetallic nanoparticles (Au-AgNPs), poly(L-Cysteine) (P(L-Cys)) and electrochemically reduced graphene oxide (ERGO) modified glassy carbon electrode (GCE/Au-AgNPs/P(L-Cys)-ERGO). The composite electrode exhibited an excellent electrocatalytic response towards NADH at a low oxidation potential (+ 0.35 V) and minimization of surface contamination due to the synergistic effects of the Au-AgNPs, polymer and ERGO. Under optimum conditions, modified sensors allowed the detection of NADH with a wide linear range from 0.083 μM to 1.05 mM with a low detection limit of 9.0 nM (S/N = 3). Moreover, this modified electrode was also used as a sensitive ethanol biosensor, which was prepared with alcohol dehydrogenase (ADH) via glutaraldehyde, bovin serum albumin and nafion (Naf). There was a linear response for ethanol in the concentration range from 0.017 to 1.845 mM with a low detection limit of 5.0 μM (S/N = 3). The GCE/Au-AgNPs/P(L-Cys)-ERGO/ADH/Naf electrode can be successfully used for the determination of ethanol in different commercial beverages.

1. Introduction

Dihydronicotinamide adenine dinucleotide (NADH) and nicotinamide adenine dinucleotide (NAD^+) are vital cofactors that play a significant role in many enzymatic reactions catalysed by dehydrogenases [1,2]. They are responsible for electron transfer in biological processes, such as biosynthesis, cellular energy metabolism, aging, carcinogenesis, gene expression, mitochondrial function, calcium homeostasis, DNA repair and cell death [3,4]. Moreover, NADH is closely related to many diseases like depression, cancer, diabetes, Alzheimer's and Parkinson's [5]. Therefore, the development of sensitive and selective methods for real-time monitoring of NADH has received considerable interest in the fields of biotechnology and biomedicine. Several methods such as high performance liquid chromatography (HPLC), electrochemistry and enzymatic cycling have been used for NADH determination [6]. Traditional detection methods, such as HPLC, colorimetry and fluorometry etc., have some disadvantages, such as low selectivity, complex preparation steps and high cost [7–9]. Recently, electrochemical methods have been developed that offer a promising approach for NADH determination due to their high sensitivity, selectivity, rapid response, easy preparation and economical efficiency [10]. However, the direct oxidation of NADH at conventional electrodes, such as those of carbon and platinum, requires a high overpotential (+0.6 V to +0.8 V). More importantly, the oxidation products of NADH can be adsorbed on the electrode surface and often causes electrode poisoning [1,11]. The modification of electrodes with many types of materials, such as nanoparticles, nanomaterials, bimetallic nanoparticles, metal complexes, redox dyes, quinones and conducting polymers, has been suggested to avoid such undesirable phenomena and to increase the selectivity of NADH electrochemical detection [12,13].

Among the metal nanoparticles, noble metal nanoparticles (Ag, Au, Pt etc.) have been proposed to construct different types of electrochemical sensors and biosensors because of their excellent properties, such as high electrocatalytic activity, good conductivity, small dimensional size, effective mass transport and biocompatibility [2,12,14].

Recently, the use of bimetallic nanoparticles has attracted much attention thanks to their enhanced activity and selectivity because of their different structure and electronic properties from their monometallic component [15]. Bimetallic nanoparticles can be prepared using different chemical and electrochemical methods. However, the chemical synthesis of Au-Ag bimetallic nanoparticles is very complicated because it needs the manipulation of different metal precursors, which can influence the properties of the Au-Ag nanoparticles [16]. Nevertheless, electrochemical methods are easy, quick, highly sensitive, cheap and environmentally friendly compared to chemical methods. The electrodes obtained by electrochemical deposition of noble metals onto the electrode surface have excellent properties for the detection of many compounds in biological systems due to the synergistic effect that may arise between the two unique electrode materials [17].

Specifically, graphene (GR), which consists of a two dimensional (2D) planar structure of sp^2 hybridized carbon atoms, has gained great

http://dx.doi.org/10.1016/j.talanta.2017.07.073
Received 12 April 2017; Received in revised form 21 July 2017; Accepted 23 July 2017
Available online 25 July 2017

importance in rapidly developing research areas. Due to its high surface area, excellent electrical conductivity and capability of modification, graphene has also been commonly used for sensor construction [2,18–20]. Graphene oxide (GO) is an electrically insulating material because of its disrupted sp^2 hybridized carbon atom bonding network. However, electrochemically reduced graphene oxide (ERGO), which is obtained by the reduction of graphene oxide, has a high electrical conductivity thanks to its restored π-network [21]. Recently, ERGO films have been directly deposited onto the surface of the electrodes at a constant potential [22] or by cycling potential [23,24]. These methods not only allow the film thickness to be controlled, but also provide one-step electrodeposition, an easily prepared electrode and homogenous polymer film [25,26].

In recent years, modified electrodes, prepared by electropolymerization of amino acids have attracted considerable attention because of their ease of fabrication, ability to form a controllable thin film and presence of functional groups that help them form multifunctional layers [25]. L-Cys is used to modify electrodes via chemical and electrochemical techniques thanks to its functional –SH, $–NH_2$ and –COOH groups [27].

In this study, the construction of highly sensitive amperometric NADH sensors is described with Au-AgNPs/P(L-Cys)/ERGO on a GCE electrode. The fabrication steps of the modified electrode are shown in Scheme 1. The Au-AgNPs/P(L-Cys)/ERGO composite was easily prepared and characterized by SEM, XPS, CV and EIS techniques. This modified electrode exhibited excellent electrocatalytic oxidation to NADH at a low potential with a wide linear range, a low detection limit and good reproducibility. Additionally, the obtained electrode was used to determine the amount of ethanol in a commercial non-alcoholic beverage and whisky, with high recovery rates.

2. Experimental

2.1. Chemicals and apparatus

NAD^+, NADH, Nafion®117 solution, alcohol dehyrogenase from Baker's yeast in the form of lyophilized powder (ADH, EC 1.1.1.1, 337 U mg^{-1}), glutaraldeyde, bovine serum albumine, $AgNO_3$, ethanol, glucose, potassium chloride, AA and DA were purchased from Sigma. UA, urea, thiourea, glucose and L-cysteine were supplied by Fluka. Hydrogen tetrachloroaurate (III) trihydrate ($HAuCl_4{\cdot}3H_2O$) was obtained from Acros Organics (Thermo Fischer Scientific, USA). GO was produced from natural graphite powder by a modified Hummers method according to ref [28], and it was kindly supplied by Dr. Bülent Zeybek (Dumlupınar University, Department of Chemistry, Turkey). All chemicals and reagents used in this work were analytical grade and used as received without further purification.

The morphologies of the modified electrodes were observed on a scanning electron microscope (SEM, FEI Nova NanoSEM 650, The Netherlands). The surface states of the nanomaterials were analysed by X-ray photoelectron spectroscopy (XPS, PHI 5000 Versa Probe spectrophotometer equipped with an Al KαX-ray source (1486.6 eV)). The Ag3d, Au4f and C1s XPS spectra were measured with 0.1 eV steps and multiplex scan fitting was accomplished with Gauss–Lorentzian functions. All electrochemical measurements were conducted using an Autolab PGSTAT 302 N electrochemical analyser which included a three-electrode voltammetric cell (Bioanalytical Systems, Inc., USA). The cell consisted a bare/modified GCE (working electrode, 3.0 mm diameter), an Ag/AgCl reference electrode (BAS MF2052) and a platinum wire counter electrode (BAS MF1032).

The electrochemical experiments were carried out in a 0.1 M phosphate buffer solution (pH 7.0). Cyclic voltammetry (CV) was performed in the potential window from −0.2 to 1.0 V at a scan rate of 50 V s^{-1}. The EIS measurements were recorded in the frequency range between 100 kHz and 0.01 Hz with 5.0 mV amplitude at an open-circuit potential (E_{OCP}). The analysis of the impedance spectra and fitting of the experimental results to equivalent circuits were carried out using Nova 11.1 software. All electrochemical measurements were conducted at room temperature.

2.2. Preparation of modified electrodes

Firstly, the GC electrode was polished with 0.05 μm alumina powder, and then washed thoroughly with ethanol and ultrapure water. After which, it was sonicated to remove the alumina residues from its surface. The modification of the GCE was performed in three steps. In the first step, the Au-AgNPs were co-electrodeposited on the surface of the GCE with a 0.01 M H_2SO_4 solution containing 0.6 mM $AgNO_3$ and 0.6 mM $HAuCl_4$ for 10 cycles in the potential range from –0.2 to +1.2 V at a scan rate of 50 mVs^{-1} [17]. For stabilizing the $AgNO_3$, 0.02 M thiourea was added into the electrochemical cells. In the second step, the Au-AgNPs modified GCE (GCE/Au-AgNPs) was coated with poly(L-cysteine) (P(L-Cys)) via the electropolymerization technique in a 0.2 M PBS (pH 7.40) containing 5.0 mM L-Cystein by CV with the potential from −1.0 V to +2.2 V for 20 cycles with a scan rate of 100 mV s^{-1} [29]. Finally, the ERGO film was electrodeposited onto the surface of the GCE/Au-AgNPs/P(L-Cys) electrodes via electroreduction of GO in a 0.1 M PBS containing 1.0 mg mL^{-1} GO and 0.1 M KCl dispersion with magnetic stirring and N_2 bubbling by cyclic voltammetry cycling between +0.60 V and −1.5 V at a scan rate of 25 mV s^{-1} for 10 cycles [25]. The GCE/Au-AgNPs/P(L-Cys)/ERGO electrode was washed with ultrapure water and allowed to air dry. For the preparation of the ADH enzyme electrode, 10 μL of enzyme solution containing BSA (1.0%), GA

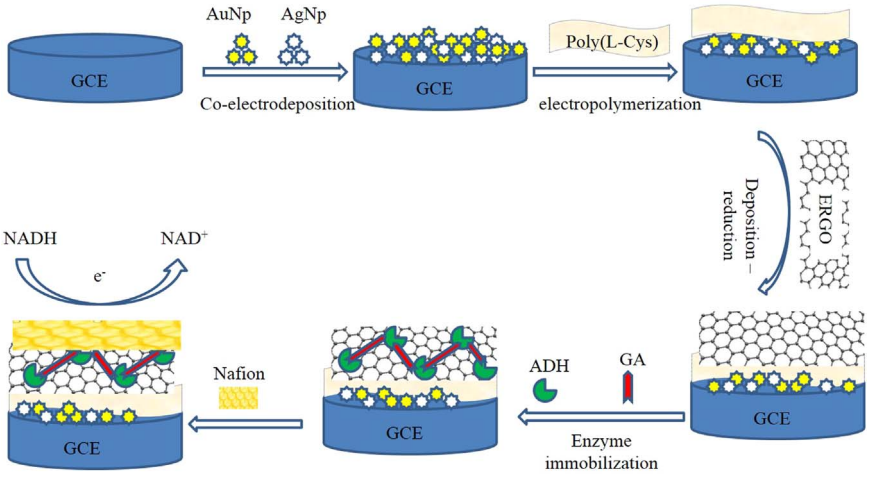

Scheme 1. Schematic illustration of the stepwise ethanol biosensor fabrication process.

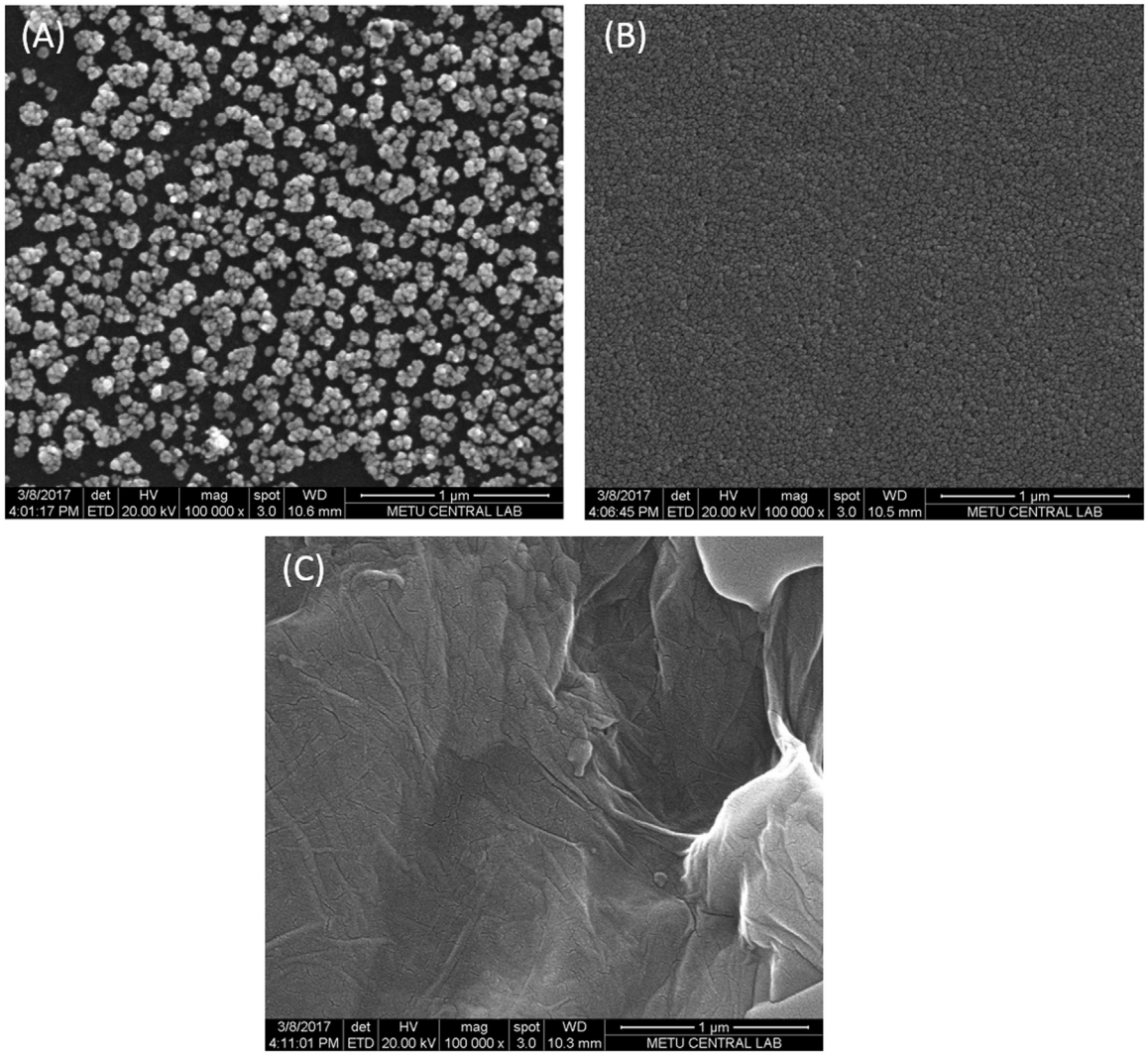

Fig. 1. SEM images of (a) GCE/Au-AgNPs, (b) GCE/Au-AgNPs/P(L-Cys) and (c) GCE/Au-AgNPs/P(L-Cys)/ERGO electrodes.

(1.25%) and 19 units of ADH (0.1 M PBS, pH 7.0) was dropped onto a GCE/Au-AgNPs/P(L-Cys)/ERGO electrode. Then, 2.0 µL of the Nafion solution (0.1%) was spread to the electrode surface and it was kept at +4.0 °C for 1 h. The prepared enzyme electrodes were stored in a refrigerator until they were used.

3. Results and discussion

3.1. Characterization of modified electrodes

To investigate the morphology and microstructure, SEM micrographs of the modified electrodes' surfaces were taken. Fig. 1 shows the SEM images of the GCE/Au-AgNPs (a), GCE/Au-AgNPs/P(L-Cys) (b) and GCE/Au-AgNPs/P(L-Cys)/ERGO electrodes (c). Fig. 1(a) reveals that the nano-sized Au-Ag nanoparticles were successfully co-deposited on the GCE surface by the CV technique. Fig. 1(b) shows that the P(L-Cys) is formed on the GCE/Au-AgNPs electrode and most of the Au-AgNPs were covered by the P(L-Cys) layer. Compared with the SEM images of the GCE/Au-AgNPs/P(L-Cys), it can be seen that the ERGO film with a wrinkled paper-like structure was obtained on the surface of the electrode. This indicates that the GO has been successfully electroreduced on the surface of the GCE/Au-AgNPs/P(L-Cys) (Fig. 1(c)).

The formation of the Au-AgNPs/P(L-Cys)/ERGO was confirmed by the XPS analysis. Fig. 2 shows the survey XPS spectrum (A) and the high-resolution XPS spectra of Au4f (B), Ag3d (C) and C1s (D) for the GCE/Au-AgNPs/P(L-Cys)/ERGO electrode as well as C1s (E) for the GCE/Au-AgNPs/P(L-Cys)/GO electrode. The results of the XPS survey spectrum showed C1s, N1s, S2s, S2p, Ag3d3, Ag3d5, Ag3p1, Ag3p3, Au4d3, Au4d5, Au4f5 and Au4df7 peaks and confirmed the composition of the Au-AgNPs/P(L-Cys)/ERGO. In the Au4f XPS expanded spectrum, two peaks were centered at 84.05 eV and 87.72 eV, which correspond to the binding energies of $Au4f_{7/2}$ and $Au4f_{5/2}$, respectively [30]. The high resolution spectrum of Ag3d revealed two peaks at 367.22 eV ($Ag3d_{5/2}$) and 373.23 eV ($Ag3d_{3/2}$), which confirm the existence of silver in the Ag^0 form [31]. These results demonstrated that Au-AgNPs were succesfully co-reduced onto the surface of GCE. The high resolution C1s spectrum for the Au-AgNps/P(L-Cys)/GO composite displays three peaks of GO at 282.7, 284.85 and 286.54 eV, which correspond to C–C/C=C, C–O/C–N and O–C=O, respectively [32]. After electrochemical reduction, the C/O ratio increased considerably in the Au-AgNps/P(L-Cys)/ERGO composite demonstrating that a majority of the oxygenated functional groups were reduced [33].

EIS is an effective method for providing useful information on the impedance changes of the electrode surface during the construction process. The impedance spectrum known as a Nyquist plot includes a semicircle portion that corresponds to the electron transfer limited processes at high frequencies and its diameter is equal to the electron transfer resistance value (R_{et}). Meanwhile, the linear part at low

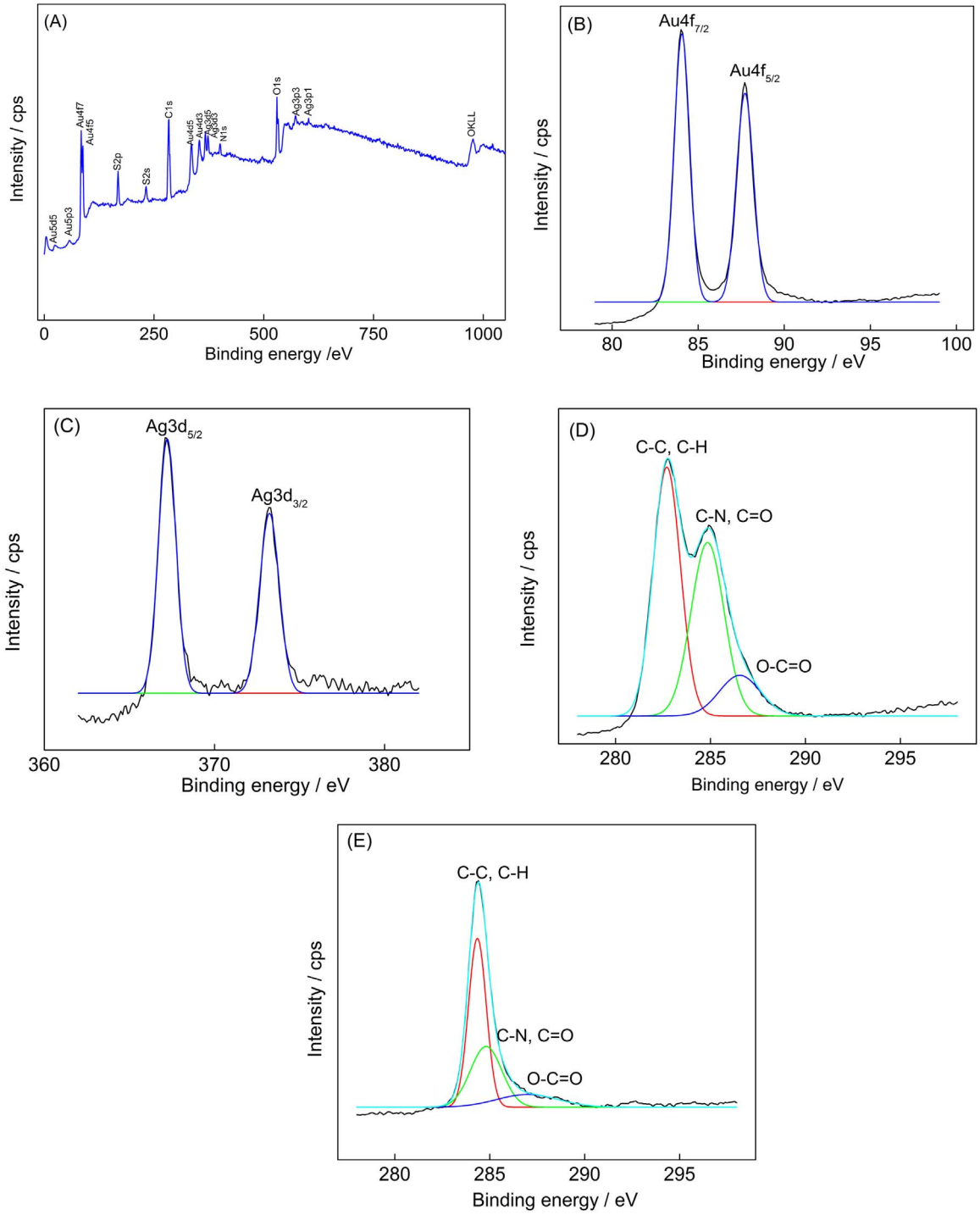

Fig. 2. XPS survey spectrum (A), the high resolution spectra of Au4f (B) and Ag3d (C) for the GCE/Au-AgNPs/P(L-Cys)/ERGO electrode. XPS spectra of C1s for the GCE/Au-AgNPs/P(L-Cys)/GO (D) and GCE/Au-AgNPs/P(L-Cys)/ERGO (E).

frequencies corresponds to the diffusion control impedance of the ions [34]. Fig. S1 shows the Nyquist plots of the BGCE (curve a) and the modified electrodes (curve b-f) in 0.1 M KCl containing 5.0 mM $Fe(CN)_6^{3-/4-}$. It can be seen from Fig. 3 that the R_{et} value of the bare GCE (curve a) (1550 Ω) decreased when the electrode surface was modified with Au-AgNPs (curve b) (122 Ω). The reason could be attributed to the large surface area and high surface free energy of the Au-AgNPs [35]. When the GCE/Au-AgNPs electrode was modified with P(L-Cys) (curve c), the R_{et} value decreased to 76.5 Ω, and the reason could be due to the fast electron transfer ability of the P(L-Cys) [36]. The R_{et} value obtained at the GCE/Au-AgNPs/P(L-Cys)/ERGO electrode (23.3 Ω) was much lower than that of the GCE/Au-AgNPs and GCE/Au-AgNPs/P(L-Cys). This could be mainly attributed to the electrical conductivity of the ERGO [37]. These results indicated that the Au-AgNPs, P(L-Cys) and ERGO could serve as an efficient electron transfer pathway between the surface of the electrode and the electrolyte solution.

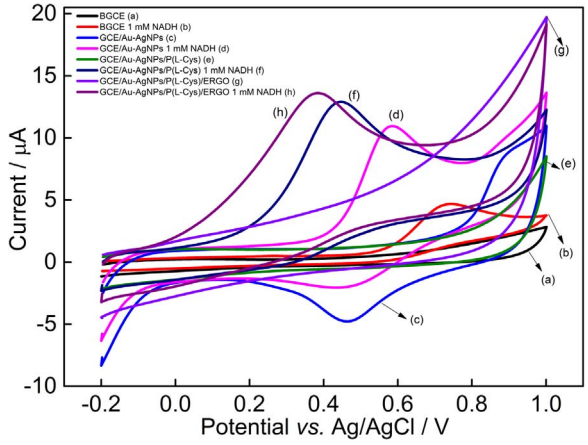

Fig. 3. Cyclic voltammograms of the bare GCE (a, b), GCE/Au-AgNPs (c, d), GCE/Au-AgNPs/P(L-Cys) (e, f) and GCE/Au-AgNPs/P(L-Cys)/ERGO (g, h) in 0.1 M PBS (pH 7.0) without and with 1.0 mM NADH, respectively.

3.2. Electrochemical behaviour of NADH at different modified electrodes

The electrochemical response of NADH was examined using the CV technique. Fig. 3 displays the cyclic voltammograms at the bare GCE (a,b), GCE/Au-AgNPs (c,d), GCE/Au-AgNPs/P(L-Cys) (e,f) and GCE/Au-AgNPs/P(L-Cys)/ERGO (g,h) in 0.1 M PBS (pH 7.0) with a scan rate of 50 mV s^{-1} without and with 1.0 mM NADH, respectively. The electro-oxidation peak of the NADH at the bare GCE was observed at +0.73 V in the potential range from –0.2 V to +1.0 V. Meanwhile, the oxidation peak potential of NADH at the GCE/Au-AgNPs electrode shifted to 0.574 V and the peak current increased two-fold compared to the bare GCE. When the GCE/Au-AgNPs surface was modified by P(L-Cys), an obvious decrease in the peak potential and an increase in the current response were obtained in comparison with the GCE/Au-AgNPs. Among all these modified electrodes, the highest peak current was observed at the GCE/Au-AgNPs/P(L-Cys)/ERGO and the lowest electro-oxidation potential of NADH was at about 0.372 V. This reduction in the overpotential may be attributed to the high electrical conductivity, electrocatalytic effect and synergistic action of Au-AgNPs, P(L-Cys) and ERGO, which provide the low-potential determination of NADH.

3.3. Effect of scan rate on peak current

To understand the reaction mechanism, the effect of the scan rate of the potential sweep on the peak current of the NADH was investigated using the CV technique. Fig. S2 shows the cyclic voltammograms at the GCE/Au-AgNPs/P(L-Cys)/ERGO electrode in 0.1 M PBS (pH 7.0) containing 1.0 mM NADH. The oxidation peak currents of the NADH increased and the peak potential shifted positively with increasing scan rate (inset of Fig. S2). Fig. S2 indicates that the electron transfer reaction was controlled by the diffusion of the NADH [3,38]. The linear relationship between the oxidation peak current of NADH and the square root of the scan rate was obtained with the following equation: I_{pa} (μA) = 11.43 $v^{1/2}$ $(Vs^{-1})^{1/2}$ + 2.88 (R^2 = 0.994).

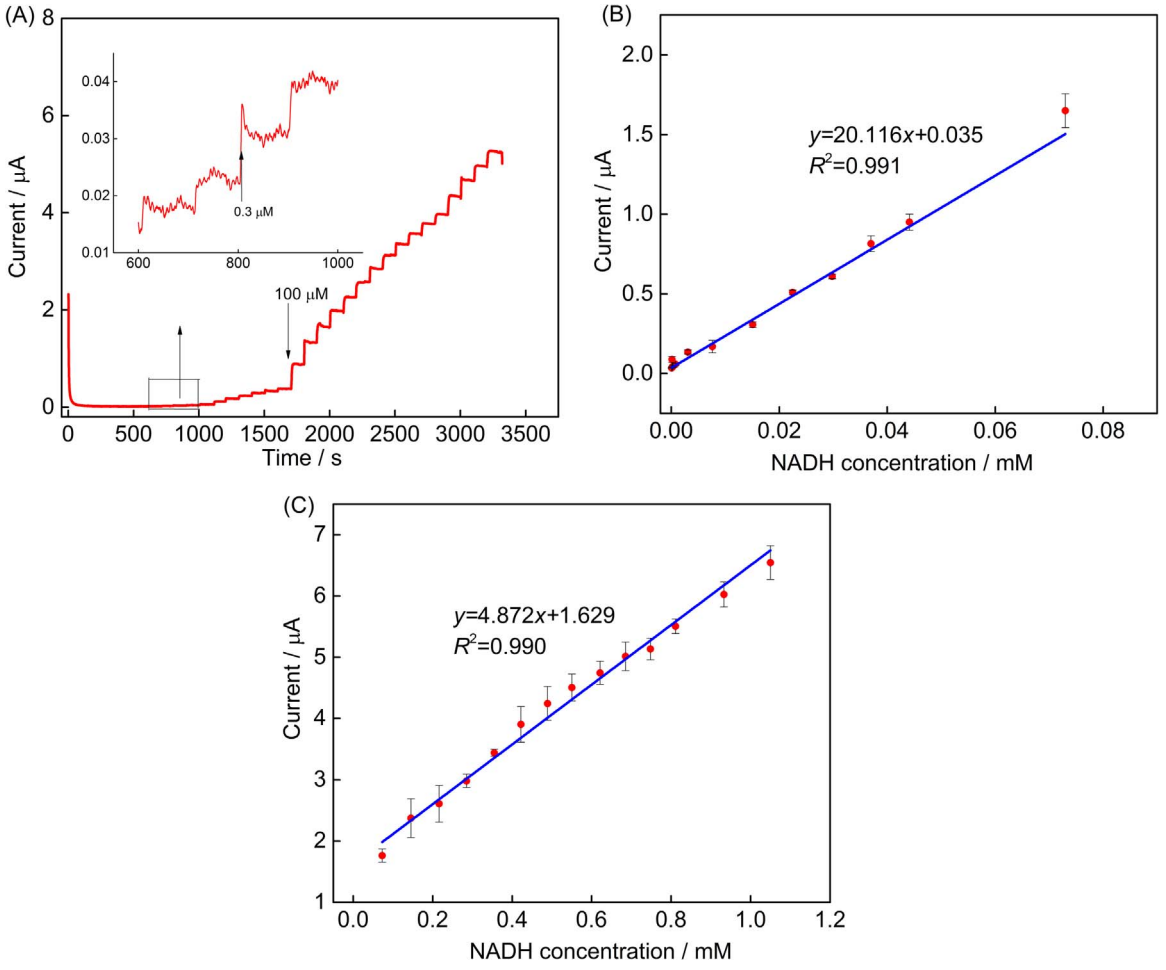

Fig. 4. Chronoamperometric responses of GCE/Au-AgNPs/P(L-Cys)/ERGO in PBS (0.1 M, pH 7.0) on successive addition of different NADH concentrations at applied potential of + 0.35 V (vs. Ag/AgCl) (A). Calibration plots of chronoamperometric current response versus NADH concentration at GCE/Au-AgNPs/P(L-Cys)/ERGO (B) and (C).

The effect of the operating potential on the current response of the GCE/Au-AgNPs/P(L-Cys)/ERGO electrode was examined in the potential range from +0.1 V to +0.4 V. Fig. S3 displays the chronoamperometric response of the NADH at different applied potentials under continuous stirring. As can be seen in Fig. S3, a very low response was obtained for a potential of +0.1 V; whereas there was an obvious increase in the oxidation current from +0.1 V to +0.3 V and the current reached a maximum value at +0.4 V. However, the oxidation currents of the NADH slightly increased with an increase in the potential from + 0.35 to + 0.4 V. The linear calibration plots at different working potentials are also shown in Fig. S3 (inset). Based on the CV and chronoamperometric studies, the working potential was selected as +0.35 V for the following experiments.

3.4. Amperometric detection of NADH on GCE/Au-AgNPs/P(L-Cys)/ERGO

Fig. 4 (A) exhibits the chronoamperometric responses of the GCE/Au-AgNPs/P(L-Cys)/ERGO towards NADH oxidation in 0.1 M PBS (pH 7.0) under stirring at the working potential of +0.35 V vs. Ag/AgCl. As can be seen in Fig. 4 (A), the current increased and reached 95% of the stable state within approximately 3 s following each addition of NADH. Two calibration graphs were shown in Fig. 4 (B) and (C). The proposed sensor response displayed two linear concentration ranges; one from 0.083 to 73.0 μM with a linear regression equation of I (μA) = 0.035 + 20.116 c_{NADH} (mM) (R^2 = 0.991) and sensitivity of 20.116 μA mM^{-1} and another one from 73.0 μM to 1.05 mM with a linear regression equation of (μA) = 1.629 + 4.872 c_{NADH} (mM) (R^2 = 0.990) and sensitivity of 4.872 μA mM^{-1}. The detection limit was determined to be 9.0 nM (S/N = 3). A comparison of the linear working range and detection limit of the modified electrode with the previously reported NADH sensing systems [1–3,39–45] is shown in Table 1. The developed sensor presented in this study could result in a better analytical performance in terms of the linear dynamic range, detection limit and applied potential. This could be attributed to the co-electrodepositon of Ag and Au nanoparticles, which could establish a synergistic effect with the P(L-Cys) and ERGO.

3.5. Stability, reproducibility and interference study

To investigate the stability of the composite electrode, the amperometric response of this electrode was measured in the presence of 1.0 mM NADH at an applied potential of 0.35 V over 1000 s. Fig. 5 indicates that the response of the GCE/Au-AgNPs/P(L-Cys)/ERGO electrode was maintained at 91% of its first response, whereas that of the bare electrode decreased by more than 67% of the first response

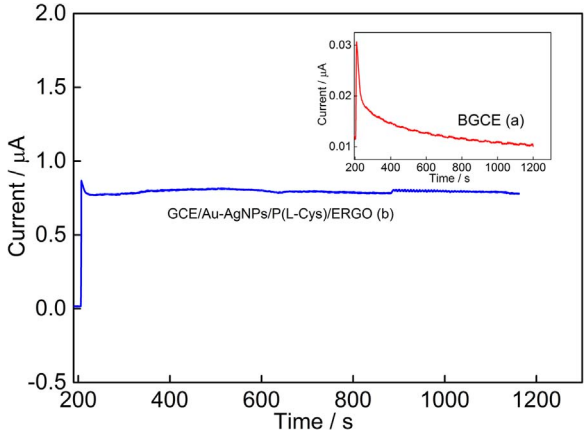

Fig. 5. Chronoamperometric recordings for 1.0 mM NADH at +0.35 V obtained at BGCE (a) and GCE/Au-AgNPs/(P(L-Cys))/ERGO (b).

throughout the experiment. The decrease in the current response of the NADH is due to the adsorption of the oxidation products of NADH on the surface of the bare electrode that causes a fouling effect [39]. The long-term stability of the modified electrode can be attributed to the anti-fouling feature of the GCE/Au-AgNPs/P(L-Cys)/ERGO electrode.

The reproducibility of the five different GCE/Au-AgNPs/P(L-Cys)/ERGO electrodes was studied by running five calibration plots in the range of 0.164–1.562 mM. The relative standard deviation (RSD) of the sensitivities was 2.2%. To investigate the repeatability of the proposed electrode, five sequential calibration graphs were plotted using the same NADH sensor. The RSD of the sensitivity value was estimated to be 1.1%. These results reveal that the developed composite electrode has good reproducibility and repeatability for the determination of NADH.

To evaluate the anti-interference ability of the GCE/Au-AgNPs/P(L-Cys)/ERGO, the effects of common interfering substances including ascorbic acid, dopamine, glucose and uric acid on the amperometric response of NADH were investigated (Fig. 6). The amperometric measurement was performed by the successive addition of NADH (1.0 mM) and the interfering compounds (1.0 mM) in 0.1 M PBS. It can be seen that the interference effects of the DA, GLU and UA were negligible for the amperometric determination of NADH. After the injection of AA, the oxidation current of NADH slightly increased (approximately 4.2%) when compared to those of the other interfering substances. This shows that the GCE/Au-AgNPs/P(L-Cys)/ERGO has a high selectivity for the determination of NADH due to the positive effect of the low operating potential.

Table 1
Comparison of analytical performances of the different modified electrodes for the determination of NADH.

Electrode	Linearity (μmol L^{-1})	LOD (μmol L^{-1})	Sensitivity (μA/μmol L^{-1})	Technique / working potential (V)	Reference
GCE/SWCNTs (oxidized)-Polytyr	0.15–83.0	0.0079	68 ± 1 (217 ± 3 μA/μmol L^{-1} cm^{-2})	Amp. / 0.200	[39]
GCE/NDG	0.5–12.0	0.37	0.16 (μA/μmol L^{-1})	Amp. / 0.490	[40]
GCE/ERGO-PTH	10–3900	0.1	143 (μA/mmol L^{-1} cm^{-2})	Amp. / 0.400	[1]
GCE/Gr-PQQ-CTS	0.32–220	0.16	0.421 (μA/μmol L^{-1} cm^{-2})	Amp. / 0.320	[3]
GC/Pt/Fe_3O_4/RGO	0.03–1.50	0.005	733 (nA/μmol L^{-1})	Amp. / 0.500	[41]
GCE/nPEDOT	5.0–45.0	3.8	26 (μA/mmol L^{-1})	Amp. / 0.500	[42]
GCE/Gr-AuNRs	20.0–160.0	6.0	10.27 (μA/mmol L^{-1} cm^{-2})	Amp. / 0.400	[43]
GCE/rGO-AuNPs	0.05–50.0	0.00113	916.0 (μA/mmol L^{-1} cm^{-2})	Amp. / 0.550	[2]
GCE/$PEDOT_{SDS}$/AgNPs/MB	10.0–560.0	0.1	2 (μA/mmol L^{-1})	Amp. / −0.05	[44]
GCE/NiONPs	0.11–1000.0	0.106	52.0 (μA/mmol L^{-1})	Amp. / 0.350	[45]
GCE/Au-AgNPs/P(L-Cys)/ERGO	0.082–73.0 / 73.0–1050.0	0.009	20.116 /4.872 (μA/ mmol L^{-1})	Amp. / 0.350	This study

glassy carbon electrode (GCE), single walled carbon nanotubes (SWCNTs), poly-tyrosine (Polytry) nitrogen doped graphene (NDG), electroreduced graphene oxide (ERGO), polythionine (PTH), pyrroloquinoline quinone (PQQ), chitosan (CTS), platinum (Pt), iron (II, III) oxide (Fe_3O_4), reduced graphene oxide (rGO), nanoporous poly(3,4-ethylene dioxythiophene), graphene (Gr), gold nanorods (AuNRs), gold nanoparticles (AuNPs), poly(3,4-ethylene dioxythiophene-sodium dodecyl sulfate) ($PEDOT_{SDS}$), Meldola's blue (MB), nickel oxide nanoparticles (NiONPs), gold-silver nanoparticles (Au-AgNPs), poly(L-cysteine) (P(L-Cys)).

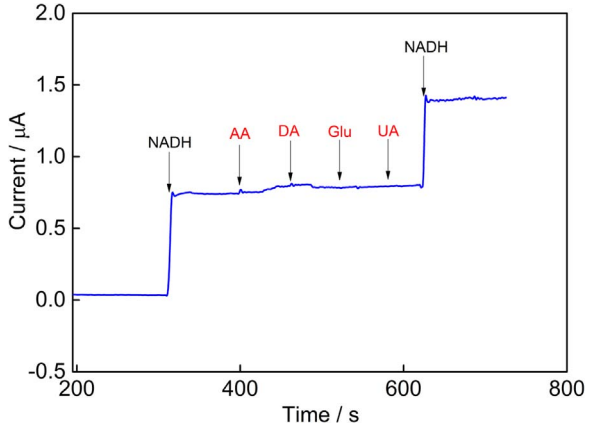

Fig. 6. Chronoamperometric response of the GCE/Au-AgNPs/P(L-Cys)/ERGO in PBS (0.1 M, pH 7.0) containing 1.0 mM NADH in the presence of potentially interfering substance with the concentration of 1.0 mM (AA, DA, Glu, UA).

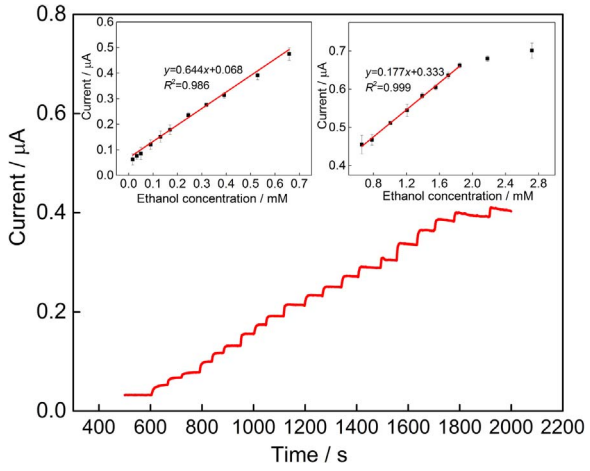

Fig. 7. Chronoamperometric response of GCE/Au-AgNPs/P(L-Cys)/ERGO/ADH/Naf in PBS (0.1 M, pH 7.0) on successive addition of different ethanol concentrations at applied potential of + 0.35 V (vs. Ag/AgCl). Inset shows a plot of chronoamperometric current response versus ethanol concentration at GCE/Au-AgNPs/P(L-Cys)/ERGO/ADH/Naf.

3.6. Amperometric biosensing of ethanol at GCE/Au-AgNPs/P (L-Cys)/ERGO

The proposed composite electrode was used as a novel dehydrogenase-based amperometric ethanol biosensing platform for the immobilization of ADH. Under the optimum conditions, the amperometric response of the GCE/Au-AgNPs/P(L-Cys)/ERGO/ADH/Naf was recorded at +0.35 V with the successive additions of ethanol in a stirred 0.1 M PBS (pH 7.0) containing 3.0 mM NAD^+ (Fig. 7). After each addition of ethanol, a stable response was obtained within 10 s. The current response increased linearly with the ethanol concentration in the range from 0.017 to 0.658 mM (0.986 × $10^{-4}\%_{vol}$–0.382 × $10^{-2}\%_{vol}$) and 0.658–1.845 mM (0.382 × $10^{-2}\%_{vol}$–0.0107%$_{vol}$) with the linear regression equations of I (μA) = 0.068 + 0.644 c_{ETOH} (mM) (R^2 = 0.986) and I (μA) = 0.333 + 0.177 c_{ETOH} (mM) (R^2 = 0.999), respectively. The sensitivities were found to be 0.644 μA mM^{-1} and 0.177 μA mM^{-1}, respectively. The limit of detection was calculated as 5 μM (0.29 ×$10^{-4}\%_{vol}$) (S/N = 3), which was lower than that of 451.6 μM, 24 μM and 2.85 mM reported for sensors based on poly-diallylmethylsilane (PDAMS)-Pt nanoparticles [46], poly(diallyldimethylammonium chloride)-covered multiwalled carbon nanotubes [47] and Clark-type transducer [48], respectively.

The reproducibility, repeatability and storage stability of the ADH biosensor were also evaluated. For reproducibility, the RSD value of sensitivities obtained with five different enzyme electrodes was calculated as 3.0%, which demonstrates the good reproducibility of the fabrication procedure. The RSD value of sensitivities for five repetitive determinations using the same electrode was 1.9%.

The storage stability of the biosensor is an important parameter for the construction of an enzyme modified electrode. The current response remained at 86% of its first response after two months storage at + 4 °C This can be attributed to the biocompatible microstructure of the Au-AgNPs/P(L-Cys)/ERGO/ADH/Naf composite that can maintain the activity of the ADH.

3.7. Real sample analysis

The fabricated biosensor was tested by using non-alcoholic beverages and whisky samples and the results were summarized in Table 2. Standard addition method was used for determination of ethanol concentration in non-alcoholic beverage spiked phosphate buffer solution. For whisky samples (containing 40% ethanol) three different concentrations were tested. The samples were assayed with the ADH biosensor and three concentrations of ethanol were calculated from the calibration curve. As can be observed, the recovery values ranged from 101.59% to 104.20%, demonstrating good accuracy for ethanol detection. The obtained results indicated that the determination of ethanol using the Au-AgNPs/P(L-Cys)/ERGO/ADH/Naf composite was effective and sensitive.

4. Conclusion

In this study, a novel electrochemical sensor was developed for the rapid, selective and sensitive determination of NADH. It can be seen that the designed Au-AgNps/P(L-Cyc)/ERGO electrode can be utilized as an excellent electron transfer mediator to shuttle electrons between the NADH and the electrode surface due to the synergistic effects inside the composite. Both of the modified electrodes, with and without the enzyme, exhibited a wide linear range, high sensitivity with a very low detection limit, good reproducibility, repeatability and high stability. Besides, the Au-AgNps/P(L-Cys)/ERGO modified GCE had a strong anti-interference ability. Furthermore, the ADH biosensor was successfully applied to NADH detection with high recovery values in real samples.

Table 2
Determination of ethanol in real samples (n = 3).

Sample	Added / mM	Expected / mM	Found / mM	RSD / %	Recovery %
Non-alcoholic beverage	0.250	–	0.256	2.1	102.40
	0.500	–	0.521	2.1	104.20
	0.750	–	0.770	1.1	102.67
Whisky	–	0.287	0.292	1.8	101.74
	–	0.378	0.384	0.3	101.59
	–	0.595	0.612	1.3	102.86

Appendix A. Supplementary material

Supplementary data associated with this article can be found in the online version at doi:10.1016/j.talanta.2017.07.073.

References

[1] Z. Li, Y. Huang, L. Chen, X. Qin, Z. Huang, Y. Zhou, Y. Meng, J. Li, S. Huang, Y. Liu, W. Wang, Q. Xie, S. Yao, Amperometric biosensor for NADH and ethanol based on electroreduced graphene oxide–polythionine nanocomposite film, Sens. Actuators B: Chem. 181 (2013) 280–287.

[2] M. Govindhan, M. Amiri, A. Chen, Au nanoparticle/graphene nanocomposite as a platform for the sensitive detection of NADH in human urine, Biosens. Bioelectron. 66 (2015) 474–480.

[3] S. Han, T. Du, H. Jiang, X. Wang, Synergistic effect of pyrroloquinoline quinone and graphene nano-interface for facile fabrication of sensitive NADH biosensor, Biosens. Bioelectron. 89 (Part 1) (2017) 422–429.

[4] H. Karimi-Maleh, A.L. Sanati, V.K. Gupta, M. Yoosefian, M. Asif, A. Bahari, A voltammetric biosensor based on ionic liquid/NiO nanoparticle modified carbon paste electrode for the determination of nicotinamide adenine dinucleotide (NADH), Sens. Actuators B: Chem. 204 (2014) 647–654.

[5] S.-J. Lin, L. Guarente, Nicotinamide adenine dinucleotide, a metabolic regulator of transcription, longevity and disease, Curr. Opin. Cell Biol. 15 (2) (2003) 241–246.

[6] R. Zadmard, P. Akbari-Moghaddam, S. Darvishi, M. Mirza-Aghayan, A highly selective fluorescent chemosensor for NADH based on calix[4]arene dimer, Tetrahedron 73 (5) (2017) 604–607.

[7] C.-H. Chen, Y.-C. Chen, M.-S. Lin, Amperometric determination of NADH with Co3O4 nanosheet modifiedelectrode, Biosens. Bioelectron. 42 (2013) 379–384.

[8] L. Deng, L. Zhang, L. Shang, S. Guo, D. Wen, F. Wang, S. Dong, Electrochemiluminescence detection of NADH and ethanol based on partial sulfonation of sol–gel network with gold nanoparticles, Biosens. Bioelectron. 24 (7) (2009) 2273–2276.

[9] Y. Dilgin, D.G. Dilgin, Z. Dursun, H.İ. Gökçel, D. Gligor, B. Bayrak, B. Ertek, Photoelectrocatalytic determination of NADH in a flow injection system with electropolymerized methylene blue, Electrochim. Acta 56 (3) (2011) 1138–1143.

[10] M. Sosna, A. Bonamore, L. Gorton, A. Boffi, E.E. Ferapontova, Direct electrochemistry and Os-polymer-mediated bioelectrocatalysis of NADH oxidation by Escherichia coli flavohemoglobin at graphiteelectrodes, Biosens. Bioelectron. 42 (2013) 219–224.

[11] Fidal V.T, Chandra T.S, New approach to biosensing of co-enzyme nicotinamide adenine dinucleotide (NADH) by incorporation of neutral red in aluminum doped nanostructured ZnO thin films, Biochim. Biophys. Acta (BBA) - General. Subj. 1861 (6) (2017) 1559–1565.

[12] H. Hamidi, B. Haghighi, Fabrication of a sensitive amperometric sensor for NADH and H2O2 using palladium nanoparticles-multiwalled carbon nanotube nanohybrid, Mater. Sci. Eng.: C. 62 (2016) 423–428.

[13] C. Creanga, N. El Murr, Development of new disposable NADH biosensors based on NADH oxidase, J. Electroanal. Chem. 656 (1–2) (2011) 179–184.

[14] K. Saha, S.S. Agasti, C. Kim, X. Li, V.M. Rotello, Gold nanoparticles in chemical and biological sensing, Chem. Rev. 112 (5) (2012) 2739–2779.

[15] K. Hareesh, R.P. Joshi, D.V. Sunitha, V.N. Bhoraskar, S.D. Dhole, Anchoring of Ag-Au alloy nanoparticles on reduced graphene oxide sheets for the reduction of 4-nitrophenol, Appl. Surf. Sci. 389 (2016) 1050–1055.

[16] C. Yuan, W. Wei, Y. Mei, X. Luo, W. Lei, A new approach for fabricating Au-Ag alloy nanoparticles confined in Al2O3 matrix, Mater. Lett. 190 (2017) 248–251.

[17] Y.-H. Chen, R. Kirankumar, C.-L. Kao, P.-Y. Chen, Electrodeposited Ag, Au, and AuAg nanoparticles on graphene oxide-modified screen-printed carbon electrodes for the voltammetric determination of free sulfide in alkaline solutions, Electrochim. Acta 205 (2016) 124–131.

[18] Y. Qian, S. Lu, F. Gao, Preparation of MnO2/graphene composite as electrode material for supercapacitors, J. Mater. Sci. 46 (10) (2011) 3517–3522.

[19] Y. Qian, S. Lu, F. Gao, Synthesis of manganese dioxide/reduced graphene oxide composites with excellent electrocatalytic activity toward reduction of oxygen, Mater. Lett. 65 (1) (2011) 56–58.

[20] M. Liu, Q. Chen, C. Lai, Y. Zhang, J. Deng, H. Li, S. Yao, A double signal amplification platform for ultrasensitive and simultaneous detection of ascorbic acid, dopamine, uric acid and acetaminophen based on a nanocomposite of ferrocene thiolate stabilized Fe3O4@Au nanoparticles with graphene sheet, Biosens. Bioelectron. 48 (2013) 75–81.

[21] O.-M. Istrate, L. Rotariu, C. Bala, Electrochemical determination of NADH using screen printed carbon electrodes modified with reduced graphene oxide and poly(allylamine hydrochloride), Microchim. Acta 183 (1) (2016) 57–65.

[22] T. Lindfors, A. Österholm, J. Kauppila, M. Pesonen, Electrochemical reduction of graphene oxide in electrically conducting poly(3,4-ethylenedioxythiophene) composite films, Electrochim. Acta 110 (2013) 428–436.

[23] S.Y. Toh, K.S. Loh, S.K. Kamarudin, W.R.W. Daud, Graphene production via electrochemical reduction of graphene oxide: synthesis and characterisation, Chem. Eng. J. 251 (2014) 422–434.

[24] H.-L. Guo, X.-F. Wang, Q.-Y. Qian, F.-B. Wang, X.-H. Xia, A. Green, Approach to the synthesis of graphene nanosheets, ACS Nano 3 (9) (2009) 2653–2659.

[25] D. Zhang, L. Li, W. Ma, X. Chen, Y. Zhang, Electrodeposited reduced graphene oxide incorporating polymerization of L-lysine on electrode surface and its application in simultaneous electrochemical determination of ascorbic acid, dopamine and uric acid, Mater. Sci. Eng.: C. 70 (Part 1) (2017) 241–249.

[26] L. Chen, Y. Tang, K. Wang, C. Liu, S. Luo, Direct electrodeposition of reduced graphene oxide on glassy carbon electrode and its electrochemical application, Electrochem. Commun. 13 (2) (2011) 133–137.

[27] K. Zhang, P. Luo, J. Wu, W. Wang, B. Ye, Highly sensitive determination of Sunset Yellow in drink using a poly (L-cysteine) modified glassy carbon electrode, analytical, Methods 5 (19) (2013) 5044–5050.

[28] T.A. Pham, J.S. Kim, J.S. Kim, Y.T. Jeong, One-step reduction of graphene oxide with l-glutathione, Colloids Surf. A: Physicochem. Eng. Asp. 384 (1–3) (2011) 543–548.

[29] Y. Gu, W. Liu, R. Chen, L. Zhang, Z. Zhang, β-Cyclodextrin-functionalized gold nanoparticles/poly(L-cysteine) modified glassy carbon electrode for sensitive determination of metronidazole, Electroanalysis 25 (5) (2013) 1209–1216.

[30] P. Wang, Z.-G. Liu, X. Chen, F.-L. Meng, J.-H. Liu, X.-J. Huang, UV irradiation synthesis of an Au-graphene nanocomposite with enhanced electrochemical sensing properties, J. Mater. Chem. A 1 (32) (2013) 9189–9195.

[31] S. Agnihotri, G. Bajaj, S. Mukherji, S. Mukherji, Arginine-assisted immobilization of silver nanoparticles on ZnO nanorods: an enhanced and reusable antibacterial substrate without human cell cytotoxicity, Nanoscale 7 (16) (2015) 7415–7429.

[32] G. Aydoğdu Tığ, G. Günendi, Ş. Pekyardımcı, A selective sensor based on Au nanoparticles-graphene oxide-poly(2,6-pyridinedicarboxylic acid) composite for simultaneous electrochemical determination of ascorbic acid, dopamine, and uric acid, J. Appl. Electrochem. (2017) 1–12.

[33] S. Woo, J. Lee, S.-K. Park, H. Kim, T.D. Chung, Y. Piao, Electrochemical codeposition of Pt/graphene catalyst for improved methanol oxidation, Curr. Appl. Phys. 15 (3) (2015) 219–225.

[34] M.I. Prodromidis, Impedimetric immunosensors—a review, Electrochim. Acta 55 (14) (2010) 4227–4233.

[35] X. Ren, X. Meng, F. Tang, Preparation of Ag–Au nanoparticle and its application to glucose biosensor, Sens. Actuators B: Chem. 110 (2) (2005) 358–363.

[36] B. Regis, L. Ferraz, F. Roberto, F. Leite, A.R. Malagutti, Simultaneous determination of ethionamide and pyrazinamide using poly(L-cysteine) film-modified glassy carbon electrode, Talanta 154 (2016) 197–207.

[37] M. Yun, J.E. Choe, J.-M. You, M.S. Ahmed, K. Lee, Z. Üstündağ, S. Jeon, High catalytic activity of electrochemically reduced graphene composite toward electrochemical sensing of orange II, Food Chem. 169 (2015) 114–119.

[38] J. Balamurugan, T.D. Thanh, N.H. Kim, J.H. Lee, Facile fabrication of FeN nanoparticles/nitrogen-doped graphene core-shell hybrid and its use as a platform for NADH detection in human blood serum, Biosens. Bioelectron. 83 (2016) 68–76.

[39] M. Eguílaz, F. Gutierrez, J.M. González-Domínguez, M.T. Martínez, G. Rivas, Single-walled carbon nanotubes covalently functionalized with polytyrosine: a new material for the development of NADH-based biosensors, Biosens. Bioelectron. 86 (2016) 308–314.

[40] S. Mutyala, J. Mathiyarasu, A highly sensitive NADH biosensor using nitrogen doped graphene modified electrodes, J. Electroanal. Chem. 775 (2016) 329–336.

[41] M. Roushani, S.J. Hoseini, M. Azadpour, V. Heidari, M. Bahrami, M. Maddahfar, Electrocatalytic oxidation behavior of NADH at Pt/Fe3O4/reduced-graphene oxide nanohybrids modified glassy carbon electrode and its determination, Mater. Sci. Eng.: C. 67 (2016) 237–246.

[42] R. Rajaram, S. Anandhakumar, J. Mathiyarasu, Electrocatalytic oxidation of NADH at low overpotential using nanoporous poly(3,4)-ethylenedioxythiophene modified glassy carbon electrode, J. Electroanal. Chem. 746 (2015) 75–81.

[43] L. Li, H. Lu, L. Deng, A sensitive NADH and ethanol biosensor based on graphene–Au nanorods nanocomposites, Talanta 113 (2013) 1–6.

[44] A. Balamurugan, K.-C. Ho, S.-M. Chen, T.-Y. Huang, Electrochemical sensing of NADH based on Meldola blue immobilized silver nanoparticle-conducting polymer electrode, Colloids Surf. A: Physicochem. Eng. Asp. 362 (1–3) (2010) 1–7.

[45] E. Sharifi, A. Salimi, E. Shams, Electrocatalytic activity of nickel oxide nanoparticles as mediatorless system for NADH and ethanol sensing at physiological pH solution, Biosens. Bioelectron. 45 (2013) 260–266.

[46] A. Jiménez, M.P.G. Armada, J. Losada, C. Villena, B. Alonso, C.M. Casado, Amperometric biosensors for NADH based on hyperbranched dendritic ferrocene polymers and Pt nanoparticles, Sens. Actuators B: Chem. 190 (2014) 111–119.

[47] B. Kowalewska, P.J. Kulesza, Toward more efficient bioelectrocatalytic oxidation of ethanol for amperometric sensing and biofuel cell technology, Anal. Chem. 84 (21) (2012) 9564–9571.

[48] A.M. Pisoschi, A. Pop, A.I. Serban, G.P. Negulescu, Ethanol determination by an amperometric bienzyme sensor based on a Clark-type transducer, J. Electroanal. Chem. 671 (2012) 85–91.